Rahau S. Shirazi[†], Mikhail Vyssotski*[†], Kirill Lagutin[†], Dion Thompson[†], Christa MacDonald[‡], Vincent Luscombe[‡], Michelle Glass[‡], Kim Parker[§], Emma K. Gowing[§], D. Bradley G. Williams[⊥], and Andrew N. Clarkson[§]

Neuroprotective activity of new Δ3-N-acylethanolamines in a focal ischemia stroke model[1,2]

[†]Callaghan Innovation, 69 Gracefield Rd, Gracefield, Lower Hutt, New Zealand.

[‡]Department of Pharmacology, University of Auckland, Private Bag 92019, Auckland, New Zealand and Department of Pharmacology and Toxicology, University of Otago, PO Box 56, Dunedin 9054

[§]Department of Anatomy, Brain Health Research Centre and Brain Research New Zealand, University of Otago, Dunedin 9054, New Zealand

[⊥]School of Mathematical and Physical Sciences, University of Technology Sydney, PO Box 123, Broadway, Sydney, NSW 2007, Australia.

* E-mail: mikhail.vyssotski@callaghaninnovation.govt.nz

KEYWORDS. Lipids, N-acylethanolamine, NAE, ischemia, stroke, neuroprotection, nasal spray

[1] Preliminary results of the study were presented at the 6th International Conference on PLA2 and Lipid Mediators. Tokyo, 2015 (Vyssotski *et al.* 2015a)

[2] Rahau Shirazi and Mikhail Vyssotski should be considered joint first author

Neuroprotective activity of new Δ3-N-acylethanolamines in a focal ischemia stroke model[3,4]

ABSTRACT. N-acylethanolamines (NAE, also called ethanolamides) are significant lipid signalling molecules with anti-inflammatory, pain-relieving, cell-protective and anticancer properties. Here, we present the use of a hitherto unreported group of Δ3-NAE and also some Δ4- and Δ5-NAE, in *in vitro* and *in vivo* assays to gain a better understanding of their structure-bioactivity relationships. We have developed an efficient synthetic method to rapidly produce novel unlabelled and ^{13}C labelled Δ3-NAE (NAE-18:5n-3, NAE-18:4n-6) and Δ4-NAE (NAE-22:5n-6). The new NAE with shorter carbon backbone structures confer greater neuroprotection than their longer carbon backbone counterparts, including anandamide (Δ5-NAE-20:4n-6) in a focal ischemia mouse model of stroke. Our work highlights structure-dependent protective effects of new NAE following focal ischemia, in which some of the new NAE, administered intranasally, lead to significantly reduced infarct volume and improved recovery of limb use. The relative affinity of the new NAE towards cannabinoid receptors was assessed against anandamide, NAE-22:6n-3 and NAE-20:5n-3, which are known cannabinoid receptor ligands with high binding constants. Among the newly synthesized NAE, Δ4-NAE-22:5n-6 shows the greatest relative affinity to cannabinoid receptors hCB_1 and hCB_2, and inhibition of cAMP activity through hCB_2 compared to anandamide.

[3] Preliminary results of the study were presented at the 6th International Conference on PLA2 and Lipid Mediators. Tokyo, 2015 (Vyssotski *et al.* 2015a)

[4] Rahau Shirazi and Mikhail Vyssotski should be considered joint first author

List of Abbreviations

ATP	adenosine triphosphate
BSTFA	N,O-bis(trimethylsilyl)trifluoroacetamide
cAMP	cyclic adenosine monophosphate
COSY	correlation spectroscopy
FFA	free fatty acid(s)
GARP	globally optimized alternating phase rectangular pulse
GC-FID	gas chromatography with flame-ionisation detector
GC-MS	gas chromatography with mass-spectrometric detector
HSQC	^{1}H, ^{13}C heteronuclear single quantum coherence (correlation) experiment
MEM	Minimal Essential Medium
NAE	N-acyethanolamine(s)
NMR	nuclear magnetic resonance
SIM	selected ion monitoring (in mass-spectrometry)
SPE	solid phase extraction
TLC	thin-layer chromatography
TMS	tetramethylsilane

INTRODUCTION

Stroke remains one of the leading causes of death and long-term disability in adults worldwide, and the incidence of stroke is on the rise due to an aging population, certain lifestyle choices and hypertension (Dobkin, 2008). Current pharmacological treatments are restricted to thrombolytic therapies such as "tPA" (Wardlaw *et al*. 2014), which has a restricted therapeutic time window of 3–4.5 hours and is a valid treatment option only for a limited number of clinical cases, creating an urgent need for new and effective therapeutics.

Endocannabinoids and related N-acylethanolamines (NAE) have been shown to exhibit neuroprotective properties in models of ischemic stroke by modulating stroke infarct size and improving prognostic outcomes. For instance, arachidonoylethanolamide (also known as AEA, NAE-20:4n-6), and the saturated N-palmitoylethanolamine, NAE-16:0, reduce the infarct volume, reduce functional neurological deficit and reduce neuroinflammation in rats following stroke (Sinor *et al.* 2000, Garg *et al.* 2010).

Molecular targets of endocannabinoid NAE are known to include the cannabinoid receptors CB_1 and CB_2. While anandamide (NAE-20:4n-6) binds to CB_1 and CB_2 receptors and stimulates biochemical pathways such as receptor-mediated signal transduction, not all NAE share these receptor binding characteristics. Some NAE that are cannabinoid receptor-inactive (e.g. N-oleoylethanolamine and N-palmitoylethanolamine) potentiate anandamide responses through what is known as 'entourage effects' (Schmid & Berdyshev, 2002). They are thought to do so by providing alternative substrates for fatty acid amide hydrolase enzyme, which is the principal enzyme responsible for the hydrolysis of anandamide. Thus, cannabinoid receptor-inactive NAE can be catabolically related to endocannabinoids.

The structural requirements of ligands for the exhibition of bioactivity such as activation of CB_1 and CB_2 receptors in mammals have been previously explored. Structure-activity relationship studies of NAE reveal that for the n-6 set-up of double bonds, 3–5 double bonds in an intact methylene interrupted (or 'homoallylic') system are essential for strong binding and a fatty acid chain length of at least twenty carbon atoms is critical. Fewer double bonds or a shorter chain fatty acid moiety results in significantly reduced binding. The n-3 series is overall less potent at binding to CB receptors than n-6 analogues and requires at least 5 double bonds and at least twenty carbon atoms chain length to achieve relatively good binding (Sheskin *et al.* 1997). In these cases, when viewed from the carboxylic end of the molecule, the double bond system starts at least at Δ5. With the only exception of Δ4-series NAE 22:6n-3, synaptamide (Kim & Spector, 2013), there have been no investigations into NAE systems in which the double bond system starts in the Δ3 or Δ4 system (i.e.

C3 or C4 when viewed from the carboxylic end of the compound). We were therefore interested to study such systems (i.e. Δ3- and Δ4-based NAE, in combination with n-3 and, especially n-6 methylene-interrupted double bond systems in an appropriate biological model. As far as can be determined, only two naturally existing Δ3 polyunsaturated fatty acids have been reported so far, which is indicative of their scarcity in organisms. One of them is octadecapentaenoic acid, 18:5n-3, a product of β-oxidation of eicosapentaenoic acid, with elevated levels found in some microalgae (e.g., Kuklev *et al.* 1992), and the other is a shorter chain analogue of arachidonic acid, namely γ-stearidonic acid, 18:4n-6 (found in low levels in a thermophilic cyanobacterium *Tolypothrix* sp) (Řezanka *et al.* 2012).

We hypothesized that the presence of a Δ3 double bond system in which the n-3 or n-6 pattern in the structure of the NAE is retained, in combination with a shorter than usual carbon chain, may induce a distinctive set of biological activities arising from the shorter chain. While not the focus of the present study, a key part of our thinking was that these unusual NAE may also avoid the pro-inflammatory metabolic by-products of anandamide. To the best of our knowledge, no NAE with the proposed structure (i.e. PUFA-based Δ3-NAE) has been previously synthesised and assayed. We therefore developed an efficient procedure to synthesise a series of new NAE, including unlabelled and ^{13}C labelled Δ3-NAE (NAE-18:5n-3, NAE-18:4n-6) and Δ4-NAE-22:5n-6. NAE-18:4n-6 was selected because it possesses the same n-6 four-double-bond pattern as anandamide but with the first double bond being found at the unusual Δ3 position. Here, we report on the neuroprotective properties of the new Δ3- and Δ4-NAE compared with a known Δ4-NAE (NAE-22:6n-3) and Δ5-NAE (anandamide, and NAE-20:5n-3). We show that NAE with shorter carbon backbones (NAE-18:4n-6 and NAE-18:5n-3) afford greater neuroprotection in a model of focal ischemia than anandamide or endocannabinoids with longer carbon backbone structure. We then probed their ability to interact with hCB_1 and hCB_2, to assess their potential to act as cannabinoids.

Materials and Methods

Materials. All reagents and materials were obtained from Sigma-Aldrich unless otherwise specified. Organic solvents were either of analytical or spectroscopic grade and used as received. For biological studies, anandamide was purchased from Sigma-Aldrich. TLC plates, 10 × 10 cm glass backed HPTLC Silica gel 60 plates (Merck, Germany), were activated at 110 °C for at least 90 min and left to cool to room temperature in a vacuum desiccator prior to sample loading. Free fatty acid of 18:5n-3 and 18:4n-6 were produced as described before by Vyssotski *et al*. (2015b). Caco-2 cells were purchased through Sigma-Aldrich.

NAE synthesis: The general approach used was as follows: to free fatty acid (FFA) (0.036 - 0.088 mmol) in dry chloroform (0.2 mL) was added a solution of 1,8-bis(dimethylamino)naphthalene ('proton sponge', 2.0 equiv.) in chloroform (0.2 mL) at room temperature under argon. The mixture was cooled in an ice-water bath for 10 minutes before a solution of N,N'-dicyclohexylcarbodiimide (1 equiv.) in dry chloroform (0.35 mL) was added with additional mixing. Once TLC analysis in *n*-hexane-acetone (1:1, by v/v) confirmed consumption of the FFA starting material, non-labelled or 2-^{13}C ethanolamine (1.1 equiv.) in chloroform (0.35 mL) was added and the mixture stirred at room temperature for 3 h. The mixture was filtered to remove N,N'-dicyclohexylurea before being extracted with 1 M aqueous HCl (3 × 1 mL), saturated aqueous NaCl (2 × 1 mL), with saturated aqueous $NaHCO_3$ (2 × 1 mL) and twice more with saturated NaCl solution (2 × 1 mL). The organic phase was dried over anhydrous sodium sulphate (Na_2SO_4), followed by removal of the organic solvent under a stream of argon. The residue was purified by low pressure column chromatography on silica gel 60 (230-400 mesh) with chloroform-methanol (98:2, v/v) as eluent. The solvent was removed for selected fractions under a stream of argon at 30 °C. The residues were subjected to vacuum overnight to remove residual solvents, affording the desired NAE product. Alternatively, the residue was dissolved in hexane and was purified using silica-based SPE (strata silica 70 Å, 55 µm, 1 g/6 mL, from Phenomenex), using chloroform-methanol (98:2, v/v) as eluent to yield NAE solutions as a colourless liquids. The target compounds were concentrated in a stream of argon at 30 °C and brought to constant weight *in vacuo*. R_f values using n-hexane - acetone (1:1, v/v) as eluent were consistently between 0.43–0.45. NAE were produced in 40–90% yield. This process particularly resulted in generation of ^{12}C- and/or ^{13}C-labelled NAE-(18:5n-3 and 18:4n-6) without any visible *cis-trans* or Δ3 to Δ2 double bond isomerization, as confirmed by NMR spectroscopy. GS-MS analysis was employed to confirm purity.

General process for derivatization of NAE for GC-FID and GC-MS analysis. To 1 mg of synthetic NAE was added 60 µL of BSTFA (N,O-bis(trimethylsilyl)trifluoroacetamide), followed by incubation at 60 °C for 30 min. The reaction mixture was dried under a stream of argon at 55 °C, and the residue was dissolved in hexane (2 mL) prior to analysis by GC-FID. Mouse brain samples were extracted and analysed as described in *Mouse brain uptake* section below.

Mouse brain uptake. The samples (30–50 mg of brain tissue, stored at –80 °C until analysis) were collected after 1, 3 and, in some cases, 7 h following intranasal administration of ^{13}C labelled NAE. Brain tissue was homogenized in chloroform/methanol (1:2, v/v, 1 mL), stirred and centrifuged. The supernatant was collected in a separate vial. Chloroform/methanol (1:2, v/v, 1 mL) was added to the residual matter, which was homogenised, stirred and centrifuged. The supernatants were combined and 10% aqueous KCl (1 mL) was added to the combined supernatant, which was centrifuged to

obtain phase separation. The bottom phase was collected, evaporated under a stream of argon and re-dissolved in chloroform (0.5 mL)., The ^{13}C labelled NAE was separated and derivatized as described by Muccioli & Stella (2008) prior to GC-MS analysis. Derivatized samples were analysed using GCMS-QP2010 Ultra (Shimadzu) GCMS equipped with Rtx5ms (30 m x 0.25 mm i.d., 0.25 µm stationary phase) capillary column (Restek, USA). Helium was used as carrier gas. The oven temperature program started at 150 °C (hold for 2 min), followed by a ramping to 320 °C at a rate of 4 °C/min, and maintained for 15 min. Detection was performed in selected ion monitoring (SIM) mode. The presence and amount of ^{13}C NAE-18:4n-6 was monitored using m/z 377 ion at 25.25 min, and that of ^{13}C NAE-18:5n-3 using m/z 375 ion at 25.4 min.

NMR spectroscopy. The general method and program were done following previous work by Vyssotski *et al*. (2015b). The compounds were dissolved in $CDCl_3$. ^{1}H and ^{13}C NMR spectra were obtained on a Bruker Avance–III 500 Spectrometer equipped with a Bruker 5 mm broadband probe at 303 K. Chemical shifts were referenced to internal tetramethylsilane (TMS) at 0.00 ppm. The ^{1}H and ^{13}C frequencies were 499.8 and 125.7 MHz, respectively, and 90° pulses 13.0 and 14.0 µs, respectively. The chemical shifts are reported in ppm on scale downfield from the internal standard, TMS. Signal patterns are indicated using the followings; s = singlet, d = doublet, dd = doublet of doublet, dt = doublet of triplet, t = triplet, q = quartet, qd = quartet of doublet, m = multiplet, b = broad. Standard Bruker supplied NMR pulse programs were used for recording all spectra. The pulse program COSYGPMFQF was used to record the gradient selected absolute value proton homonuclear double quantum filtered COSY spectrum. The phase-sensitive gradient-selected pulse program HSQCETGP was used for the two-dimensional (2D) inverse detected ^{1}H, ^{13}C heteronuclear (HSQC) spectra with isotropic proton mixing. Parameters for the ^{1}H spectrum were: spectral width 10,302 Hz, 65,536 data points, 30° excitation pulse and 32 transients taken, each with a 1-s delay time and acquisition time of 3.18 s. Spectra were processed with a standard exponential weighting function with a 0.3-Hz line broadening before Fourier transformation. Parameters for the WALTZ ^{1}H decoupled ^{13}C spectrum were: 30° excitation pulse, spectral width 31,250 Hz, 65,536 data points and 4,192 transients each taken with a 0.5 s delay time and acquisition time of 1.05 s for a total acquisition time of 2 h. Spectra were processed with a standard exponential weighting function with 5 Hz line broadening before Fourier transformation. Parameters for the proton homonuclear double quantum filtered COSY spectrum were as follows: two transients, each taken with a delay time 1.69 s and acquisition time 0.46 s, spectral width F2 2,222 Hz in 2,048 data points and spectral width F1 2,222 Hz in 320 slices for a total acquisition time of 25 min. The absolute value spectrum was processed with a sine bell window function in both directions. Parameters for the HSQC spectrum were: 16 scans, each taken for 320 slices in the indirect dimension with a delay time 0.96 s and

acquisition time 0.46 s, spectral width F2 2,212 Hz in 1,024 real points, sweep width F1 3,142 Hz in 512 slices and MLEV17 mixing at 8.3 kHz for 60 ms. ^{13}C GARP decoupling (globally optimized alternating phase rectangular pulse) was at 3.8 kHz during acquisition for a total acquisition time of 2 h. Data were processed with a squared cosine bell window function in both directions. All NMR data were processed using Bruker TopSpin 3.5 Pl7. ChemDraw Professional 17.0 (PerkinElmer Informatics, Inc., U.S.A.) was employed to predict ^{1}H- and ^{13}C-NMR spectra of the target compounds.

Cytotoxicity. Caco-2 cells, obtained directly from American Tissue Culture Collection (ATCC HTB-37), were maintained at 70% confluency in MEM media supplemented with 10% FCS and 100 IU/mL penicillin/streptomycin in a stationary CO_2 incubator at 37 °C. Caco-2 cells are human adenocarcinoma cells derived from human colon cancer. They were selected as this cell lines are often used as a model intestinal cell for adsorption studies and for cytotoxicity studies for ingested compounds. Cytotoxicity assays were performed within 7 passages of the ATCC stocks, by seeding 96 well plates at 5×10^4 cells per well and incubating overnight to allow the cells to adhere to the plate surface. Tests for mycoplasma contamination were not performed due to the low passage number. Samples were prepared as stock solutions in media with 10% FCS, diluted appropriately to give a 100-fold concentration range and added directly to the wells without replacing the media. Cytotoxicity was assessed 24 h later by measuring ATP luminescence (ATPLite, PerkinElmer). Curcumin and chlorambucil were used as cytotoxicity controls to monitor assay performance. Curcumin is cytotoxic and has an IC_{50} of 10–40 µg/mL for regularly used mammalian cell lines, while chlorambucil under normal cell culture conditions is only mildly cytotoxic but will change cytotoxicity if conditions such as media pH changes or if the cells become confluent.

Animals and protocols. All procedures described in this study were carried out in accordance with guidelines on the care, and use of laboratory animals set out by the University of Otago, Animal Ethics Committee (AEC #42/11 and AEC #119/15) and the Guide for Care and Use of Laboratory Animals (NIH Publication No. 85–23, 1996), and in accordance with the ARRIVE guidelines. Male C57BL/6J mice (2–3 months old; 28–32 g) were housed under a 12 h light/dark cycle with ad libitum access to food and water. An n=5 animals per group were assessed for all studies and n=10 for data relevant to vehicle (infarct volume analysis and behavioural tasks).

Drug treatments. Intranasal administration of the NAE was chosen because this method allows rapid absorption and transport of the compounds into the brain without enzymatic degradation. Intranasal administration was performed using a plastic cone with its end cut off. Mice were placed into the plastic cone to restrain the mouse and to gain access to their noses. Using a pipette and a 100 µL pipette tip, 50 µL of vehicle or drug was drop wise applied onto the tip of the nose / nostrils

(delivered over a 30–60 second period), and the mice were allowed to inhale and absorb the solution. All drugs were suspended in either ethanol or DMSO and then diluted with deionized H_2O to reach the desired drug dosing of 0.1, 1 or 10 mg/Kg for all the compounds tested.

Photothrombosis. Focal stroke was induced by photothrombosis (Clarkson *et al*. 2010; Clarkson *et al*. 2011). Under isoflurane anaesthesia (2–2.5% in O_2) 2–4-month-old adult C57BL/6J male mice were placed in a stereotactic apparatus, the skull exposed through a midline incision, cleared of connective tissue and dried. A cold light source (KL1500 LCD, Zeiss) attached to a 40× objective giving a 2 mm diameter illumination was positioned 1.5 mm lateral from Bregma, and 0.2 mL of Rose Bengal solution (10 g/L in normal saline, i.p.) was administered. After 5 minutes, the brain was illuminated through the intact skull for 15 minutes to induce stroke. Following the light exposure, the skin was closed using surgical glue, and the mice returned to their home cage maintained on a heating blanket until they had fully recovered from the anaesthesia and could be returned to their holding rooms.

Behavioural assessment. Animals were tested once on both the grid-walking and cylinder tasks, one week prior to surgery to establish baseline performance levels. For all the studies, animals were tested one-week post-stroke at approximately the same time of day at the end of their dark cycle. All behaviours were scored by observers who were blind to the treatment group of the animals in the study (Clarkson *et al*. 2010; Clarkson *et al*. 2011). An n=5 animals per group were assessed on all behavioural tasks. Following all behavioural studies, mice were sacrificed, and brains processed to quantify the volume of infarction.

Grid-walking test. The grid-walking apparatus was manufactured using 12 mm square wire mesh with a grid area 32 cm / 20 cm / 50 cm (length / width / height). A mirror was placed beneath the apparatus to allow video footage in order to assess the animals' stepping errors (i.e., 'foot-faults'). Each mouse was placed individually atop of the elevated wire grid and allowed to freely walk for a period of 5-minutes. During this 5-minute period, the total number of foot-faults for each limb along with the total number of non-foot-fault steps were counted and a ratio between foot-faults and total steps taken calculated. Percent foot-faults were calculated by: [#foot-faults / (#foot-faults + #non-foot-fault steps) * 100]. To take into account differences in the degree of locomotion between animals and trials, a ratio between foot-faults and total steps taken was used.

Cylinder task. The spontaneous forelimb task encourages the use of forelimbs for vertical wall exploration / press in a cylinder. When placed in a cylinder, the animal rears to a standing position, whilst supporting its weight with either one or both of its forelimbs on the side of the cylinder wall. A cylinder 15 cm in height with a diameter of 10 cm is used. Videotape footage of animals in the

cylinder was evaluated quantitatively in order to determine forelimb preference during vertical exploratory movements. While the video footage was played in slow motion (1/5th real time speed), the time (sec) during each rear that each animal spent on either the right forelimb, the left forelimb, or on both forelimbs were calculated. Only rears in which both forelimbs could be clearly seen were timed. From these three measures, the total amount of time spent on either limb independently as well as the time the animal spent rearing using both limbs was derived. The percentage of time spent on each limb was calculated and these data were used to derive a spontaneous forelimb asymmetry index (% ipsilateral use / % contralateral use). The 'contact time' method of examining the behaviour was chosen over the 'contact placement' method, as it takes into account the slips that often occur during a bilateral wall press post-stroke.

Infarct size. At seven days post-stroke animals were anesthetized, transcardially perfused with 4% paraformaldehyde and brains extracted and processed histologically using cresyl violet staining in order to quantify infarct volume as previously described (Clarkson *et al.* 2013; Bix *et al.* 2013). Stroke volume was calculated as per the equation:

$$\text{Infarct volume } (mm^3) = \text{Area } (mm^2) \times \text{Section Thickness (mm)} \times \text{Section Interval}$$

Binding and functional assays. Experiments utilized human CB_1, or CB_2 tagged at the N-terminus with three haemagglutinin sequences (HA-hCB_1, HA-hCB_2) stably transfected into HEK 293 as previously described (Cawston *et al.* 2013; Grimsey *et al.* 2011). HEK 293 were cultivated in Dulbecco's Modified Eagle's Medium (DMEM) supplemented with 10% foetal bovine serum (FBS) and zeocin, (250 µg/mL). Cells were maintained in 5% CO_2 at 37 °C in a humidified atmosphere. Cells were grown in 75 mm^2 flasks and passaged when 80–90% confluent. Cells are maintained for no more than 25 passages following thaw. Cells are routinely screened for mycoplasma utilising a mycoplasma detection kit (iNtRON Biotechnology (Seoul, South Korea); cat# 25237)

Binding assays. HEK 293-hCB_1 or HEK293-hCB_2 cells were grown to 90–100% confluence in 175 cm^2 flasks and harvested in ice-cold phosphate-buffered saline with 5 mM EDTA. Cells were centrifuged at 200 × g for 10 minutes and the pellet frozen at −80 °C until required. Pellets were thawed with Tris-sucrose buffer (50 mM Tris-HCl, pH 7.4, 200 mM sucrose, 5 mM $MgCl_2$, 2.5 mM EDTA) and homogenized with a glass homogenizer. The homogenate was centrifuged at 1000 × g for 10 minutes at 4 °C and the pellet discarded. The supernatant was then centrifuged at 27 000 × g for 30 minutes at 4 °C. The final pellet was resuspended in a minimal volume of Tris-sucrose buffer, and aliquoted then stored at −80 °C. Protein concentration was determined using the DC protein assay kit (Bio-Rad, Hercules, CA, USA) following the manufacturer's protocol. Membranes (1020 µg/point) were resuspended in binding buffer (50 mM HEPES, 1 mM MgCl2, 1 mM CaCl2, 0.2% (w/v) bovine serum

albumin (BSA, ICP Bio, New Zealand, pH 7.4) and incubated with [^{3}H]-CP55940 (2.5 nM) (PerkinElmer, Waltham, MA, USA) and a range of NAE concentrations at 30 °C for 60 minutes in the presence of 200 nM URB597. GF/C Harvest Plates (PerkinElmer) were pre-soaked in 0.1% polyethyleneimine and then washed with 200 µL ice-cold wash buffer (50 mM HEPES, pH 7.4, 500 mM NaCl, 0.1% BSA) prior to filtration of samples, which were then subjected to additional washes (3 × 200 µL) in ice-cold wash buffer. Harvest plates were dried overnight at 24 °C, after which scintillation fluid (50 µL) was added to each well and plates were read 30 minutes later for 2 minutes per well in a Microbeta Trilux (PerkinElmer). Equilibrium binding assays were performed in triplicate, repeating assays for each mediator 3 or more times. Data were analysed using GraphPad Prism; curves are generated using a One site – fit Ki Competitive Binding function with Kd of [^{3}H]-CP55,940 constrained to 2.5 nM at hCB_1 and 2.0 nM at hCB_2.

cAMP measurement. Cellular cAMP levels were measured as previously described (Cawston *et al*. 2013). Briefly, cells are plated in 10 cm dishes and transfected approximately 24 hours later, when in log phase of growth at approximately 50% confluency. The pcDNA3L-His-CAMYEL plasmid (ATCC, Manassas, VA, USA) was transfected into HEK 293-hCB_1 cells using linear polyethyleneimine (MW 25 kDa) (Polysciences, Warrington, PA, USA). 24 h after transfection cells were re-plated in poly-D-lysine (0.05 mg/mL in phosphate buffered saline) coated white CulturPlate™-96 (PerkinElmer) at a density of 80,000 cells per well. After 24 h, cells were serum-starved in Hank's balanced salt solution containing 1 mg/mL BSA, pH 7.4 for 30 minutes prior to assay. Five minutes prior to the addition of drug or vehicle dissolved in Hank's balanced salt solution plus 1 mg/mL BSA cells were treated with 5 µM Coelenterazine-h (Promega, Madison, WI, USA). Emission signals were detected simultaneously at 460\25 nm (RLuc) and 560\25 nm (YFP), immediately following drug addiction with a Victor-Lite plate reader (PerkinElmer) at 37 °C. For concentration response curves an area under the curve analysis was carried out across the first 20 minutes of cAMP stimulation and normalized to forskolin (100%) and vehicle (0%) and plotted as a sigmoidal concentration response curve in GraphPad Prism.

Statistical methods. All data are expressed as mean ± standard error of the mean. For behavioural testing, differences between treatment groups were analysed using two-way ANOVA with repeated measures and Newman–Keuls' multiple pair-wise comparisons for post hoc comparisons. The level of significance was set at <0.05. An n=5 animals per group were assessed for all studies and n=10 for data relevant to vehicle (infarct volume analysis and behavioural tasks). For behavioural experiments, six animals per group are required to achieve > 80% power (86% calculated), considering the following parameters: $\alpha = 0.05$; with an effect size = 1.5. For histological experiments, five animals per group are required to achieve > 80% power (91% calculated), considering the following parameters: $\alpha = 0.05$; effect size 1; three concentrations; two groups, and

correlation between measures = 0.5. Parameters were determined from our prior work, in which we have demonstrated significant behavioural effects, and on the assumption that variance was about 25%. Power calculations were performed with G Power Software (version 3.1.5).

Results.

NAE synthesis. Compounds tested in the current study are presented in Figure 1. A convenient synthesis of the free fatty acid 18:4n-6 has been published recently (Vyssotski *et al.* 2015b), and 18:5n-3 was produced by using the same approach. To synthesise NAE of Δ3 polyunsaturated fatty acids, namely 18:4n-6 and 18:5n-3, a variety of bases tried led to formation of both the desired product and its *trans*-Δ2 isomer. Only 1,8-bis(dimethylamino)naphthalene allowed the successful synthesis of the NAE without isomerization. The remaining NAE were readily synthesized from the corresponding free fatty acids using the same method, resulting in efficient production of NAE-22:5n-6, NAE-20:4n-6, NAE-22:6n-3, and NAE-20:5n-3. NAE-18:4n-6 was obtained with the yield of 6.5 mg (0.020 mmol, 59%), and purity of 93.6% (by GC-FID and GC-MS), while its labelled analogue, ^{13}C NAE-18:4n-6 was obtained with the yield of 13 mg (0.041 mmol, 59%) and 95.8% purity (by GC-FID and GC-MS). Similarly, NAE-18:5n-3 was produced with the yield of 8 mg (0.025 mmol, 93%), and purity 92.5% (by GC-FID and GC-MS) , while its labelled analogue, ^{13}C NAE-18:5n-3, was obtained with the yield of 12.1 mg (0.038 mmol, 51%), and 98.9% purity (by GC-FID and GC-MS). Chemical shifts of novel NAE as determined by ^{1}H- and ^{13}C-NMR experiments are presented in Figure 2, and also as follows:

NAE-18:4n-6: ^{1}H NMR ($CDCl_3$, 500 MHz): δ = 0.89 (t, *J* =7, 3H, CH_2-C**H**$_3$), 1.31-1.38 (broad m, 6H, CH_2-C**H**$_2$), 2.06 (q, 2H, C**H**$_2$-C=), 2.84 (m, 6H, =CC**H**$_2$C=), 3.08 (d, 2H, C**H**$_2$-CO), 3.41 (q, 2H, C**H$_2$**-N), 3.72 (t, 2H, C**H**-O), 5.38 (m, 6H, C=C**H**), 5.61 (m, 1H, C=C**H**), 5.69 (m, 1H, C=C**H**), 6.14 (b, 1H, N-**H**); ^{13}C NMR ($CDCl_3$, 125 MHz): δ = 14.03, 22.55, 25.65, 25.69, 27.22, 29.29, 31.50, 35.08, 42.56, 62.40, 122.03, 126.99, 127.41, 127.51, 128.88, 129.09, 130.62, 133.18, 172.02.

^{13}C NAE-18:4n-6: ^{1}H NMR ($CDCl_3$, 500 MHz): δ = 0.89 (t, , 3H, CH_2-C**H**$_3$), 1.30-1.36 (broad m, 6H, CH_2-C**H**$_2$), 2.05 (q, 2H, C**H**$_2$-C=), 2.84 (m, 6H, =CC**H**$_2$C=), 3.07 (d, 2H, C**H**$_2$-CO), 3.41 (dq, 2H, C**H**$_2$-N, $J_{C\text{-}H}$ = 137.9 Hz), 3.71 (t, 2H, C**H**-O), 5.38 (m, 6H, C=C**H**), 5.60 (m, 1H, C=C**H**), 5.69 (m, 1H, C=C**H**), 6.14 (b, 1H, N-**H**); ^{13}C-NMR ($CDCl_3$, 125 MHz): δ = 14.04, 22.55, 25.66, 27.22, 29.29, 31.51, 35.08, 42.58, 62.41 (d, $J_{C\text{-}C}$ = 38.3 Hz), 122.07, 127.01, 127.41, 127.52, 128.88, 129.08, 130.62, 133.11, 171.94.

NAE-18:5n-3: yield 8 mg (0.025 mmol, 93%). Purity 92.5% (by GC-FID and GC-MS). ^{1}H NMR ($CDCl_3$, 500 MHz): δ = 0.98 (t, *J* =7, 3H, CH_2-C**H**$_3$), 2.07 (qui, 2H, CC**H**$_2$-C), 2.83 (m, 8H, =C-C**H**$_2$C=), 3.08 (d, 2H, C**H**$_2$CON), 3.42 (q, 2H, C**H**$_2$-N), 3.71 (t, 2H, C**H**$_2$-OH), 5.38 (m, 8H. **H**C=C**H**), 5.59 (m, 1H, **H**C=CH), 5.68

(m, 1H, **H**C=CH), 6.14 (b, 1H, N-**H**); ^{13}C NMR ($CDCl_3$, 125 MHz): δ = 14.24, 20.56, 25.55, 25.64, 25.70, 35.08, 42.56, 62.37, 122.07, 126.98, 127.06, 127.76, 128.56, 128.70, 129.01, 132.10, 133.11, 171.96.

^{13}C NAE-18:5n-3: yield 12.1 mg (0.038 mmol, 51%). Purity 98.9% (by GC-FID and GC-MS). ^{1}H NMR ($CDCl_3$, 500 MHz): δ = 0.98 (t, *J* =7, 3H, CH_2-C**H**$_3$), 2.07 (qui, 2H, CC**H**$_2$-C), 2.83 (m, 8H, =C-C**H**$_2$C=), 3.08 (d, 2H, C**H**$_2$CON), 3.41 (dq, $J_{C\text{-}H}$ = 138 Hz, 2H, C**H**$_2$-N), 3.71 (t, 2H, C**H**$_2$-OH), 5.38 (m, 8H, **H**C=C**H**), 5.59 (m, 1H, **H**C=CH), 5.68 (m, 1H, **H**C=CH), 6.14 (b, 1H, N-**H**); ^{13}C NMR ($CDCl_3$, 125 MHz): δ = 14.24, 20.56, 25.56, 25.66, 35.08, 42.58, 62.41 (d, $J_{C\text{-}C}$ = 38.6 ^{13}C-N), 122.09, 126.98, 127.07, 127.76, 128.56, 128.70, 129.01, 132.10, 133.09, 171.95.

NAE are not cytotoxic in vitro. The cytotoxicity of two NAE were assessed on a human colon cell line (Caco-2) in vitro. The NAE showed only moderate toxicity with both NAE having similar IC_{50} values (70–80 μg/mL, 220-250 μM) as shown in Table 1 and Figure 3. Of particular note, the concentrations that showed moderate levels of toxicity are two to three orders of magnitude higher than the concentrations required for hCB_1 or hCB_2 inhibition.

Short carbon-backbone NAE decrease infarct size. Previous studies have reported the neuroprotective effects of NAE after stroke (e.g., Sinor *et al*. 2000, Garg *et al*. 2010). Not all types of stroke have a reperfusion component, so we investigated the protective effects of several newly synthesized NAE in a photothrombosis model of stroke that has minimal reperfusion. Strokes were induced in the mouse motor cortex resulting in damage to sensory forelimb and hind limb cortical areas as well as primary forelimb and hind limb cortical areas (Clarkson *et al*. 2013). Assessment of the protective effects (infarct volume, Figure 4) of NAE administered intranasally one hour post-stroke, were undertaken one week post-stroke following motor functional/behavioural assessment.

NAE-18:4n-6 showed the most significant decrease in infarct volume out of all NAE tested compared to stroke + vehicle-treated controls ($F(3,21)=9.212$, $P=0.0004$: control: 4.62 ± 0.51 mm^3 *vs*. 2.17 ± 0.78 mm^3 at 0.1 mg/kg, $P<0.01$; 1.07 ± 0.03 mm^3 at 1 mg/kg, $P<0.001$; or 2.71 ± 0.26 mm^3 at 10 mg/kg:, $P<0.01$). Treatment with NAE-18:5n-3 also showed a significant decrease in infarct volume, following intranasal administration of the highest concentration ($F(3,21)=6.060$, $P=0.0039$: 1.38 ± 0.19 mm^3 at 10 mg/kg, $P<0.01$) compared to stroke + vehicle-treated controls (4.62 ± 0.51 mm^3). Intranasal administration of NAE-22:5n-6 ($F(3,21)=0.2059$, $P=0.8913$) and NAE-22:6n-3 ($F(2,17)=4.803$, $P=0.0106$) with longer carbon backbone structures showed minimal protection for the lowest dose (0.1 mg/kg), but no protection was observed for the middle and highest doses compared with stroke + vehicle-treated controls when given one hour post-stroke ($P>0.05$). To further investigate the effect of chain length on protection we assessed NAE with intermediate carbon backbones, namely, NAE-20:5n-3 and anandamide (NAE-20:4n-6). NAE-20:5n-3 and

anandamide both showed a statistically insignificant degree of decrease in infarct volume at the lowest dose when tested at 0.1 mg/kg ($F(3,21)=0.6494$, $P=0.5921$: 2.94 ± 0.82 mm3, $P=0.0924$; and $F(3,21)=0.2771$, $P=0.8413$: 3.58 ± 1.21 mm3, $P=0.3629$, respectively).

These data indicate that NAE with shorter carbon backbone structures afford greater protection than their longer carbon backbone structured counterparts. Taken together, the data indicate that there is a structure-dependent physiological influence following ischemia.

Short carbon-backbone NAE protect against loss of motor function. Motor functional / behavioural recovery following photothrombosis stroke was assessed on both the grid-walking and cylinder / forelimb asymmetry tasks (Clarkson *et al*. 2010; Clarkson *et al*. 2011), one week post stroke (Figure 5). The number of foot-faults relative to total steps taken (both right-forelimb and hind limb) on the grid-walking test pre-stroke and one week post-stroke is presented in the left column of Figure 5. The spontaneous forelimb asymmetry (decrease in relative time spent on the left paw relative to right) in the cylinder task in pre-stroke and one week post stroke is presented in the right column of Figure 5. There was a significant increase in the number of foot-faults (both right-forelimb and hind limb) on the grid-walking test and an increase in spontaneous forelimb asymmetry (decrease in relative time spent on the right forelimbs) in the cylinder task, one week post-stroke, compared baseline measurements. Intranasal administration of NAE-18:4n-6 (0.1, 1, or 10 mg/kg) one hour after stroke, resulted in a significant decrease in the number of forelimb foot-faults for all three concentrations tested compared with vehicle treated stroke control. It also resulted in a significant improvement in the use of the impaired right forelimb compared to vehicle treated controls, at 1 and 10 mg/kg.

The results for NAE-18:4n-6 (Figure 5a and Figure 5b in blue), NAE-18:5n-3 (Figure 5c and Figure 5d in red), NAE-22:5n-6 (Figure 5e and Figure 5f in green), NAE-22:6n-3 (Figure 5g and Figure 5h in pink), NAE-20:5n-3 (Figure 5i and Figure 5j in purple), and NAE-20:4n-6, anandamide (Figure 5k and Figure 5l in grey) are presented for three concentrations of 0.1 mg/kg, 1 mg/kg, 10 mg/kg compared with all vehicle treated stroke control (red dashed bars). All significant decreases compared to the relevant vehicle are marked. In the case of NAE-18:5n-3 (1 and 10 mg/kg, but not 0.1 mg/kg), also introduced by intranasal administration one hour after stroke, there was also a significant decrease in the number of forelimb foot faults for all three concentrations tested compared with vehicle treated stroke control (Figure 5c). At 10 mg/kg this resulted in a significant improvement in the use of the impaired right forelimb compared to vehicle treated controls.

Similar to the infarct data, intranasal administration of NAE-22:6n-3 (0.1, 1, or 10 mg/kg), failed to show any effects on behavioural recovery on either the grid-walking or cylinder tasks, compared

with vehicle treated stroke control. Furthermore, the intermediate NAE, namely, NAE-20:5n-3 and anandamide (NAE-20:4n-6) showed a small yet non-significant decrease in the number of foot-faults on the grid-walking task and improvement of forelimb asymmetry in the cylinder task compared with vehicle treated stroke control. These data further support our findings that short-carbon backbone NAE afford greater protection and improvement in motor functional recovery after stroke.

Detection of NAE in the brain following intranasal administration. Selected ion monitoring GC-MS analysis of mouse brain tissue revealed that ^{13}C NAE-18:4n-6, a labelled version of the most active NAE, administered intranasal quickly reaches the cortex, both in a healthy/sham and a stroke brain model. The compound disappeared from healthy brain 3 hours after administration, whereas it was still present in stroke brain even 7 hours after administration. In fact, the data show a rapid accumulation of the NAE and its sustained presence in the stroke brain, over the test period, especially in the stroked cortex (Figure 6). On the contrary, the presence of the labelled version of a less active NAE-18:5n-3 in the stroked cortex was less noticeable reaching the maximum 1 hour after stroke, and gradually declining within the next few hours (data not shown).

Assessment of NAE activity on hCB_1 and hCB_2 receptors. The relative affinity towards hCB_1 and hCB_2 was measured for all NAE. Consistent with previous reports anandamide exhibited pKi of 6.8 and 6.35 at hCB_1 and hCB_2, respectively (McPartland *et al*. 2007). All NAE compounds bound to both hCB_1 and hCB_2 (Table 2) with lower affinity than anandamide. The relative affinity of the compounds for hCB_1 was NAE-20:4n-6 > NAE-20:5n-3 >NAE-22:5n-6 > NAE-22:6n-3 > NAE-18:4n-6 > NAE-18:5n-3. The relative affinity of the compounds for hCB_2 was NAE-20:4n-6 > NAE-22:5n-6 > NAE-22:6n-3 > >NAE-20:5n-3 > NAE-18:4n-6 > NAE-18:5n-3.

Endocannabinoids regulate cellular levels of cAMP through a G protein-mediated interaction with adenylyl cyclase (Matsuda 1997; Rhee *et al*. 1998). In this system, activation of hCB_1 and hCB_2 activates Gαi protein, which inhibits adenylyl cyclase, the enzyme responsible for biosynthesis of cAMP. This results in reduced levels of cAMP. Agonists of hCB_1 and hCB_2 would, therefore, lead to lower levels of cAMP.

Accordingly, all NAE compounds were tested for function at hCB_1 and hCB_2 receptors with a cyclic adenosine monophosphate (cAMP) assay at concentrations up to 10 µM. At hCB_1, anandamide caused inhibition of forskolin-mediated cAMP production (EC_{50} 142 nM). Only three of the five novel NAE compounds led to robust cAMP inhibition (see Figure 7 and Table 3). All were partial agonists compared to anandamide. At hCB_2, all compounds exhibited agonist properties. NAE-22:5n-6 and NAE22:6n-3 both demonstrated greater efficacy than NAE-18:4n-6 (52% and 39% *vs.* 33% inhibition respectively) and NAE-18:5n-3 was the least efficacious (21% inhibition). The data show that the

compounds are generally lower affinity and efficacy at hCB_1 than anandamide, but very comparable to anandamide at hCB_2. Given that 18:4n-6 had the most significant effect on infarct volume, and of the lowest affinity for and efficacy with hCB_1 and hCB_2, together with the lack of correlation between these data and the neuroprotection data above, it is unlikely that the neuroprotective effects result from pathways related to hCB_1 and hCB_2. These data rather indicate that short-carbon backbone NAE are affording protection via a non-CB1 or CB_2 mediated mechanism.

Discussion.

NAE derived from unsaturated fatty acids are readily and efficiently synthesized from commercially available starting materials. It is imperative that in the synthesis of unusual Δ3-NAE 1,8-bis(dimethylamino)naphthalene is used as base to afford high yields of product and to avoid *cis*-Δ3 to *trans*-Δ2 double bond isomerization. Of the NAE assayed, short carbon-backbone NAE afford substantial neuroprotection in a focal ischemia stroke model. We show that there is significant reduction in infarct volume and improved retention of motor function in selected cases in response to the intranasal administration of the NAE one-hour post-stroke. The results demonstrate a clear structure-protection relationship, where longer-chain NAE afford little or no neuroprotection. In contrast, non-naturally occurring shorter backbone-based NAE impart notable protection. One of our goals was to try and expand the range of structure-activity relationships reported by Sheskin *et al* (1997) to shorter- and longer-chain n-6 PUFA-based NAE, hence all novel compounds were tested for activity against cannabinoid receptors hCB_1 and hCB_2. While showing affinity for both receptors, the compounds all demonstrated approximately ten-fold lower affinity than anandamide at these receptors. In a functional receptor activity screen, the compounds with longer backbones showed greater potency and efficacy at both hCB_1, whereas both 18-carbon compounds showed minimal or no activity at hCB_1. In contrast, all compounds were agonists at hCB_2. Given the low potency of these compounds for the cannabinoid receptors, it is unlikely that the effects are mediated through CB_1 or CB_2 receptors; however further studies which investigate at the stability of the compounds *in vivo* and pharmacokinetics might shed light on whether the concentrations required are achievable *in vivo*.

Endocannabinoids are extremely potent lipid signaling molecules that are involved in the control of a multitude of bodily processes, including maintenance of brain health. NAEs are abundant in the CNS and their receptors are widely expressed by both neurons and glial cells, where they modulate brain functions involved in the pathophysiology of neurological disorders. In the brain, they have been shown to participate in the regulation of feeding behaviours, cognitive functions, mood, reward, and sleep-wake cycles, and evidence suggests that they might be therapeutically exploited as

neuroprotective agents, anti-addictive medications, anticonvulsant, and antidepressant. NAEs that are derived from PUFAs, with anandamide, formed following the breakdown of arachidonic acid (AA, 20:4n-6), being the major single endocannabinoid. NAEs are endogenous bioactive lipids involved in numerous physiological functions in mammals, including neurotransmission, reproduction, inflammation, analgesia, appetite and cytoprotection and widely expressed in mammals (Schmid & Berdyshev, 2002; Schmidt *et al*, 2012). Previous studies have shown the eicosapentaenoic acid (20:5n-3) can prevent against memory impairment, modulate inflammation and decrease infarct size following stroke (Bas et al., 2007; Okabe et al., 2011). Even though the physiological functions of NAEs are largely unknown, the classical molecular targets of NAEs are known to include the cannabinoid receptors, CB1 and CB2, which we show our novel NAE compounds act on, and the vanilloid receptor 1 (VR1) (Matsuda *et al*, 1990; Devane *et al*, 1992; Lambert *et al*, 2002).

In addition to acting on classic CB1 and CB2 receptors, endocannabinoids have been shown to manipulate membrane PUFA composition and alter the function and/or signaling of a variety of receptors, including dopaminergic, cholinergic, GABAergic and Glutamatergic receptors, as well as the Na^+/K^+ ATPase and calcium calmodulin dependent kinase (Shonesy *et al*, 2013; Malnoe *et al,* 1990; Turner *et al*, 2003; Witt & Nielsen, 1994). Recent clinical advances in the stroke field has shown that disrupting NMDA / PSD95 signalling using NA1, which dampens glutamate-mediated excitotoxicity, can improve function (Hill *et al*, 2020). In addition, recent preclinical data shows that activation of calcium calmodulin dependent kinase (Leurs *et al*, 2021) or extrasynaptic GABA receptors (Clarkson *et al*, 2019) can also afford significant motor function in animal models of stroke. Given these significant advances over recent years, target validation and validation of potential lead compounds remains a major challenge for all neurodegenerative conditions. To overcome this challenge, efficient high-throughput screening tools that can screen thousands of compounds daily (Aldewachi *et al*, 2021), have the ability to find and validate novel druggable targets and improve translatability.

These highly promising outcomes provide a useful starting point for the discovery of more potent and desperately needed stroke recovery drugs. The result of our work can ultimately serve as valuable pharmacological tool to study physiology and biochemistry of the endocannabinoid systems, with a potential practical application of developing a neuroprotective nasal spray.

Acknowledgements: We acknowledge Dr Herbert Wong (Callaghan Innovation) for his assistance with the NMR spectroscopy, and Dr Andrew Lewis (Callaghan Innovation) help in editing the manuscript. This work was supported by the New Zealand Foundation for Research, Science and Technology grant C08X0709 "High value lipids" and by the Callaghan Innovation SIF project “Novel

499 bioactives", a Sir Charles Hercus Fellowship from the Health Research Council of New Zealand (ANC)
500 and support from the School of Medical Sciences, University of Auckland (MG).

501 **Authorship.** MV conceived the idea of Δ3-NAE, prepared the first and the final drafts of the
502 manuscript, and participated in analysis of the synthetic products. RS performed the bulk of the NAE
503 syntheses and NMR analysis and composed the main part of the manuscript. KL performed the
504 synthesis, purification and analysis of precursor fatty acids. DT designed and carried out the
505 cytotoxicity assays. CM and VL and MG designed and carried out the CB1 and CB2 binding and
506 signally assays. MG also contributed to the interpretation of the data and the writing of the
507 manuscript. DBGW suggested the synthetic approach and contributed to editing of the manuscript.
508 ANC, KP, and EKG designed and carried out *in vivo* assays, with ANC contributing to the writing of the
509 manuscript and interpreting the results.

510 **Conflict of Interest**: the authors declare no conflict of interest.

References:

Aldewachi, H., Al-Zidan, R.N., Conner, M.T., Salman, M.M. (2021) High-Throughput Screening Platforms in the Discovery of Novel Drugs for Neurodegenerative Diseases. Bioengineering (Basel). 8(2):30. DOI: 10.3390/bioengineering8020030.

Bas, O., Songur, A., Sahin, O., Mollaoglu, H., Ozen, O.A., Yaman, M., Eser, O., Fidan, H., Yagmurca, M. (2007) The protective effect of fish n-3 fatty acids on cerebral ischemia in rat hippocampus. Neurochem Int. 50:548-554. DOI: 10.1016/j.neuint.2006.11.005.

Bix, G.J., Gowing, E.K., Clarkson, A.N. (2013). Perlecan Domain V Is Neuroprotective and Affords Functional Improvement in a Photothrombotic Stroke Model in Young and Aged Mice. Translational Stroke Research, 4: 515-523. DOI: 10.1007/s12975-013-0266-1

Carreau, J.P., Dubacq, J.P. (1978). Adaptation of a macro-scale method to the micro-scale for fatty acid methyl transesterification of biological lipid extracts. Journal of Chromatography A, 151: 384-390. DOI: 10.1016/S0021-9673(00)88356-9.

Clarkson, A.N., Boothman-Burrell, L., Dósa, Z., Nagaraja, R.Y., Jin, L., Parker, K., van Nieuwenhuijzen, P.S., Neumann, S., Gowing, E.K., Gavande, N., Ahring, P.K., Holm, M.M., Hanrahan, J.R., Nicolazzo, J.A., Jensen, K., Chebib, M. (2019) The flavonoid, 2'-methoxy-6-methylflavone, affords neuroprotection following focal cerebral ischaemia. J Cereb Blood Flow Metab. 39(7):1266-1282. doi: 10.1177/0271678X18755628. Epub 2018 Jan 29. PMID: 29376464

Cawston, E.E., Redmond, W.J., Breen, C.M., Grimsey, N.L., Connor, M., Glass, M. (2013). Real-time characterization of cannabinoid receptor 1 (CB1) allosteric modulators reveals novel mechanism of action. British Journal of Pharmacology, 170: 893-907. DOI: 10.1111/bph.12329

Clarkson, A.N., Huang, B.S., MacIsaac, S.E., Mody, I., Carmichael, S.T. (2010). Reducing excessive GABA-mediated tonic inhibition promotes functional recovery after stroke Nature, 468: 305-309. DOI: 10.1038/nature09511

Clarkson, A.N., López-Valdés, H.E., Overman, J.J., Charles, A.C., Brennan, K.C., Thomas Carmichael, S. (2013). Multimodal examination of structural and functional remapping in the mouse photothrombotic stroke model. Journal of Cerebral Blood Flow and Metabolism, 33: 716-723. DOI: 10.1038/jcbfm.2013.7

Clarkson, A.N., Overman, J.J., Zhong, S., Mueller, R., Lynch, G., Carmichael, S.T. (2011). AMPA receptor-induced local brain-derived neurotrophic factor signaling mediates motor recovery after stroke. Journal of Neuroscience, 31: 3766-3775. DOI: 10.1523/JNEUROSCI.5780-10.2011

Devane, W.A., Hanus, L., Breuer, A., Pertwee, R.G., Stevenson, L.A., Griffin, G., Gibson, D., Mandelbaum, A., Etinger, A., Mechoulam, R. (1992) Isolation and structure of a brain constituent that binds to the cannabinoid receptor. Science 258:1946-1949. DOI: 10.1126/science.1470919

Dobkin, B.H. (2008). Training and exercise to drive poststroke recovery. Nature Clinical Practice Neurology, 4: 76-85. DOI: 10.1038/ncpneuro0709

Garg, P., Duncan, R. S., Kaja, S. & Koulen, P. (2010). Intracellular mechanisms of N-acylethanolamine-mediated neuroprotection in a rat model of stroke. Neuroscience 166: 252-262 DOI: 10.1016/j.neuroscience.2009.11.069

Grimsey, N.L., Goodfellow, C.E., Dragunow, M., Glass, M. (2011). Cannabinoid receptor 2 undergoes Rab5-mediated internalization and recycles via a Rab11-dependent pathway. Biochimica et Biophysica Acta - Molecular Cell Research, 1813: 1554-1560. DOI: 10.1016/j.bbamcr.2011.05.010

Hill, M.D., Goyal, M., Menon, B.K., Nogueira, R.G., McTaggart, R.A., Demchuk, A.M., Poppe, A.Y., Buck, B.H., Field, T.S., Dowlatshahi, D., van Adel, B.A., Swartz, R.H., Shah, R.A., Sauvageau, E., Zerna, C., Ospel, J.M., Joshi, M., Almekhlafi, M.A., Ryckborst, K.J., Lowerison, M.W., Heard, K., Garman, D., Haussen, D., Cutting, S.M., Coutts, S.B., Roy, D., Rempel, J.L., Rohr, A.C., Iancu, D., Sahlas, D.J., Yu, A.Y.X., Devlin, T.G., Hanel, R.A., Puetz, V., Silver, F.L., Campbell, B.C.V., Chapot, R., Teitelbaum, J., Mandzia, J.L., Kleinig, T.J., Turkel-Parrella, D., Heck, D., Kelly, M.E., Bharatha, A., Bang, O.Y., Jadhav, A., Gupta, R., Frei, D.F., Tarpley, J.W., McDougall, C.G., Holmin, S., Rha, J.H., Puri, A.S., Camden, M.C., Thomalla, G., Choe, H., Phillips, S.J., Schindler, J.L., Thornton, J., Nagel, S., Heo, J.H., Sohn, S.I., Psychogios, M.N., Budzik, R.F., Starkman, S., Martin, C.O., Burns, P.A., Murphy, S., Lopez, G.A., English, J., Tymianski, M.; ESCAPE-NA1 Investigators. (2020) Efficacy and safety of nerinetide for the treatment of acute ischaemic stroke (ESCAPE-NA1): a multicentre, double-blind, randomised controlled trial. Lancet. 395(10227):878-887. doi: 10.1016/S0140-6736(20)30258-0. Epub 2020 Feb 20. PMID: 32087818

Kim, H.-Y., Spector, A.A. (2013). Synaptamide, endocannabinoid-like derivative of docosahexaenoic acid with cannabinoid-independent function. Prostaglandins Leukotrienes and Essential Fatty Acids, 88: 121-125. DOI: 10.1016/j.plefa.2012.08.002

Kuklev, D.V., Aizdaicher, N.A., Imbs, A.B., Bezuglov, V.V., Latyshev, N.A. (1992). All-cis-3,6,9,12,15-octadecapentaenoic acid from the unicellular alga *Gymnodinium kowalevskii*. Phytochemistry, 31: 2401-2403. DOI: 10.1016/0031-9422(92)83286-8

Lambert, D.M., Vandevoorde, S., Jonsson, K.O., Fowler, C.J. (2002) The palmitoylethanolamide family: a new class of anti-inflammatory agents? Curr Med Chem 9:663-674. DOI: 10.2174/0929867023370707

Leurs, U., Klein, A.B., McSpadden, E.D., Griem-Krey, N., Solbak, S.M.Ø., Houlton, J., Villumsen, I.S., Vogensen, S.B., Hamborg, L., Gauger, S.J., Palmelund, L.B., Larsen, A.S.G., Shehata, M.A., Kelstrup, C.D., Olsen, J.V., Bach, A., Burnie, R.O., Kerr, D.S., Gowing, E.K., Teurlings, S.M.W., Chi, C.C., Gee, C.L., Frølund, B., Kornum, B.R., van Woerden, G.M., Clausen, R.P., Kuriyan, J., Clarkson, A.N., Wellendorph, P. (2021) GHB analogs confer neuroprotection through specific interaction with the CaMKIIα hub domain. Proc Natl Acad Sci U S A. 2021 Aug 3;118(31):e2108079118. doi: 10.1073/pnas.2108079118.

Malnoe, A., Milon, H., Reme, C. (1990) Effect of in vivo modulation of membrane docosahexaenoic acid levels on the dopamine-dependent adenylate cyclase activity in rat retina. J Neurochem, 55: 1480–5. DOI: 10.1111/j.1471-4159.1990.tb04929.x

Matsuda, L.A. (1997). Molecular aspects of cannabinoid receptors. Critical Reviews in Neurobiology, 11: 143-166. DOI: 10.1615/CritRevNeurobiol.v11.i2-3.30

Matsuda, L.A., Lolait, S.J., Brownstein, M.J., Young, A.C., Bonner, T.I. (1990) Structure of a cannabinoid receptor and functional expression of the cloned cDNA. Nature 346:561-564. doi: 10.1038/346561a0.

McPartland, J.M., Glass, M., Pertwee, R.G. (2007). Meta-analysis of cannabinoid ligand binding affinity and receptor distribution: interspecies differences. British Journal of Pharmacology, 152: 583-93. DOI: 10.1038/sj.bjp.0707399. DOI: 10.1016/j.phytochem.2012.02.028

Muccioli, G.G., Stella, N. (2008). An optimized GC-MS method detects nanomolar amounts of anandamide in mouse brain. Analytical Biochemistry, 373: 220-228. DOI: 10.1016/j.ab.2007.09.030

Okabe, N., Nakamura, T., Toyoshima, T., Miyamoto, O., Lu, F., Itano, T. (2011) Eicosapentaenoic acid prevents memory impairment after ischemia by inhibiting inflammatory response and oxidative damage. J Stroke Cerebrovasc Dis 20:188-195. DOI: 10.1016/j.jstrokecerebrovasdis.2009.11.016.

Řezanka, T., Lukavský, J., Siristova, L., & Sigler, K. (2012). Regioisomer separation and identification of triacylglycerols containing vaccenic and oleic acids, and α-and γ-linolenic acids, in thermophilic cyanobacteria *Mastigocladus laminosus* and *Tolypothrix* sp. Phytochemistry, 78: 147-155. DOI: 10.1016/j.phytochem.2012.02.028

Rhee, M.-H., Bayewitch, M., Avidor-Reiss, T., Levy, R., Vogel, Z. (1998). Cannabinoid receptor activation differentially regulates the various adenylyl cyclase isozymes. Journal of Neurochemistry, 71: 1525-1534. DOI: 10.1046/j.1471-4159.1998.71041525.x

Schmid, H.H.O., Berdyshev, E.V. Cannabinoid receptor-inactive N-acylethanolamines and other fatty acid amides: Metabolism and function. (2002). Prostaglandins Leukotrienes and Essential Fatty Acids, 66: 363-376. Cited 95 times. DOI: 10.1054/plef.2001.0348

Schmidt, W., Schafer, F., Striggow, V., Frohlich, K., Striggow, F. (2012) Cannabinoid receptor subtypes 1 and 2 mediate long-lasting neuroprotection and improve motor behavior deficits after transient focal cerebral ischemia. Neuroscience. 227:313-26. DOI: 10.1016/j.neuroscience.2012.09.080

Sheskin, T., Hanuš, L., Slager, J., Vogel, Z., Mechoulam, R. (1997). Structural requirements for binding of anandamide-type compounds to the brain cannabinoid receptor. Journal of Medicinal Chemistry, 40: 659-667. DOI: 10.1021/jm960752x

Shonesy, B.C., Wang, X., Rose, K.L., Ramikie, T.S., Cavener, V.S., Rentz, T., Baucum, A.J. 2nd, Jalan-Sakrikar, N., Mackie, K., Winder, D.G., Patel, S., Colbran, R.J. (2013) CaMKII regulates diacylglycerol lipase-alpha and striatal endocannabinoid signaling. Nat Neurosci. 16(4):456-63. doi: 10.1038/nn.3353. Epub 2013 Mar 17.

Sinor, A. D., Irvin, S. M. & Greenberg, D. A. (2000). Endocannabinoids protect cerebral cortical neurons from in vitro ischemia in rats. Neuroscience letters 278: 157-160, DOI: 10.1016/S0304-3940(99)00922-2

Turner, N., Else, P.L., Hulbert, A.J. (2003) Docosahexaenoic acid (DHA) content of membranes determines molecular activity of the sodium pump: implications for disease states and metabolism. Naturwissenschaften, 90: 521–3. DOI: 10.1007/s00114-003-0470-z

Vyssotski, M., Lagutin, K., Shirazi, R., Glass, M., Clarkson, A. (2015a). Δ3-NAE: 2,3-Dinor Anandamide. In: The Proceedings of the 6th International Conference on PLA2 and Lipid Mediators. Tokyo, p.109.

Vyssotski, M., Lagutin, K., MacKenzie, A., Itabashi, Y. (2015b). Chemical synthesis and gas chromatographic behaviour of γ-stearidonic (18:4n-6) acid. JAOCS, Journal of the American Oil Chemists' Society, 92: 383-391. DOI: 10.1007/s11746-014-2588-x

Wardlaw, J.M., Murray, V., Berge, E., del Zoppo, G.J. (2014). Thrombolysis for acute ischaemic stroke. Cochrane Database of Systematic Reviews. 14 Jul 29 2014(7):CD000213. DOI: 10.1002/14651858.CD000213.pub3.

Witt, M.-R., Nielsen, M. (1994) Characterization of the influence of unsaturated free fatty acids on brain GABA/benzodiazepine receptor binding in vitro. J Neurochem, 62: 1432–9. DOI: 10.1046/j.1471-4159.1994.62041432.x

Table 1. Cytotoxicity of two NAE against Caco-2 colon cells, compared against curcumin and chlorambucil. Data are presented as % cell viability.

	% Cell viability [a]			
Concentration µg/mL	NAE 18:4n-6 (Standard error)	NAE 18:5n-3 (Standard error)	Curcumin (Standard error)	Chlorambucil (Standard error)
500	1% (0%)	1% (0%)	ND	116% (7%)
250	1% (0%)	1% (1%)	ND	113% (24%)
125	18% (6%)	5% (6%)	1% (0%)	106% (12%)
62.5	35% (8%)	12% (8%)	11% (1%)	108% (20%)
31.2	71% (26%)	79% (26%)	102% (5%)	123 (5%)
15.6	91% (6%)	106% (6%)	104% (4%)	96% (28%)
7.8	104% (6%)	94% (6%)	105% (3%)	87% (20%)
3.9	93% (5%)	99% (27%)	93% (3%)	95% (21%)
IC_{50}, µg/mL	66 (32)	82 (27)	43 (5)	> 500

[a] Each entry represents the mean of three independent experiments, each of which used triplicate dilutions; the errors represent the standard error of the mean for each concentration. ND = not determined.

Table 2. NAE affinity on hCB_1 and hCB_2 receptors. Data presented as pKi values ± SEM (n=3)

	NAE-20:4n-6 (Anandamide)	NAE-18:5n-3	NAE-18:4n-6	NAE-22:6n-3	NAE-22:5n-6	NAE-20:5n-3
hCB_1	6.80±0.03	5.30±0.05	5.41±0.04	5.82±0.18	6.01±0.07	5.85±0.17
hCB_2	6.35±0.02	5.33±0.05	5.56±0.06	5.96±0.06	6.24±0.09	5.88±0.06

Table 3. cAMP inhibition at hCB_1 and hCB_2. pEC_{50} and EMAX data for the ability of NAE compounds to inhibit forskolin stimulated cAMP levels. Data is mean ± SEM, n=5-7.

	NAE-20:4n-6 (Anandamide)	NAE-18:5n-3	NAE-18:4n-6	NAE-22:6n-3	NAE-22:5n-6	NAE-20:5n-3
hCB_1						
pEC_{50}	6.80±0.1	ND[a]	ND[a]	6.05±0.1	6.30±0.23	6.37±0.24
EMAX (% inhibition)	47.6±1.3	ND	6.1±0.5 (at 10 µM)[b]	29.5±4.8	41.0±3.9	35.8±2.2
hCB_2						
pEC_{50}	6.28±0.09	6.52±0.35	5.89±0.34	6.57±0.17	6.54±0.09	6.36±0.15
EMAX (% inhibition)	32.56±4.09	20.67±5.13	30.72±7.32	38.54±5.30	52.42±7.68	28.29±5.28

[a] This NAE did not reach saturation and therefore pEC_{50} could not be determined (ND).

[b] Inhibition was observed at 10 µM.

Figures

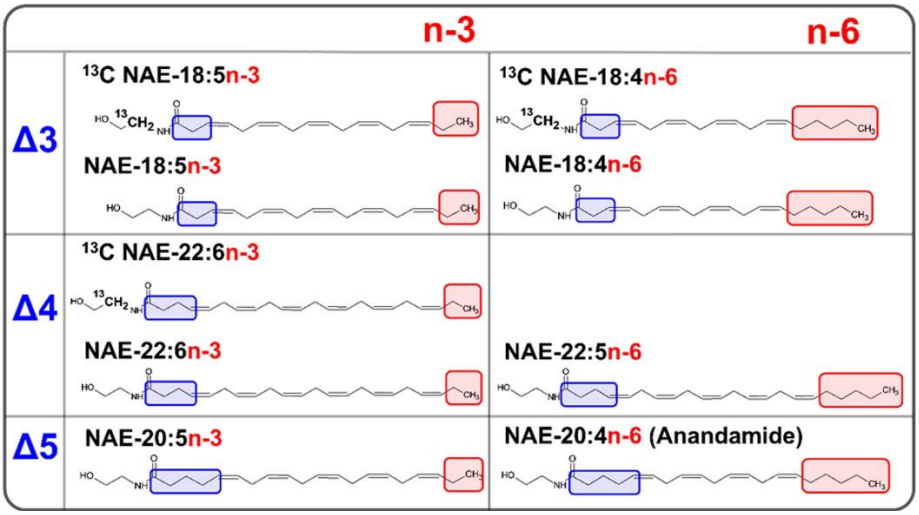

Fig. 1 Structures of the compounds used in the current study

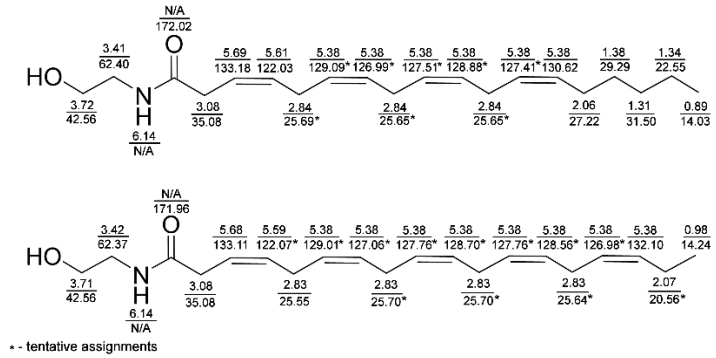

Fig. 2 ^{1}H- and ^{13}C-chemical shifts of Δ3-NAE synthesized in the current study

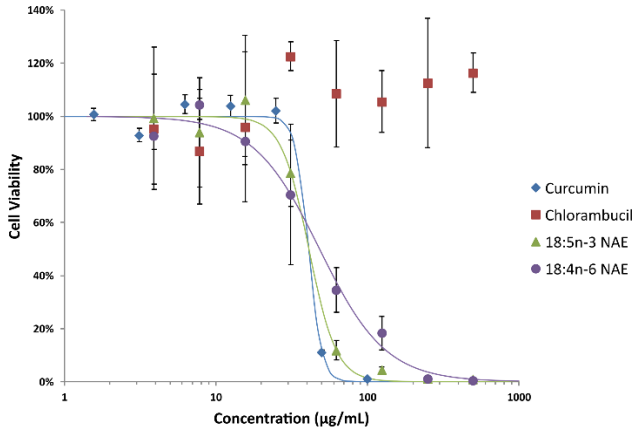

Fig. 3 Cytotoxicity of Δ3-NAE and the control chemical curcumin and chlorambucil against the Caco-2 cells (n=3, with triplicate dilutions; the error bars represent the standard error of the mean for each concentration)

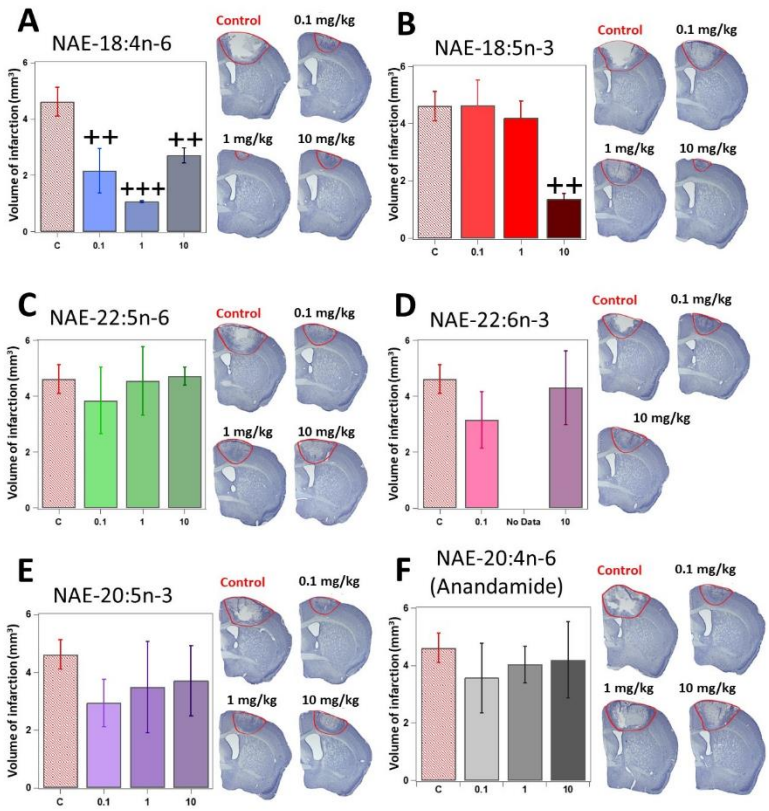

Fig. 4 Quantification of the stroke infarct volume following photothrombosis stroke and treatment with various NAE as indicated in the Figures. Data are shown as mean ± s.e.m. for n=5 animals per NAE treatment group and n=10 for the stroke + vehicle (dashed red) treatment group. Representative cresyl violet sections for each of the treatments is shown next to the quantifications for each of the NAE. Infarct has been outlined in red. ++ = P≤0.01, +++ = P≤0.001 compared to stroke + vehicle controls.

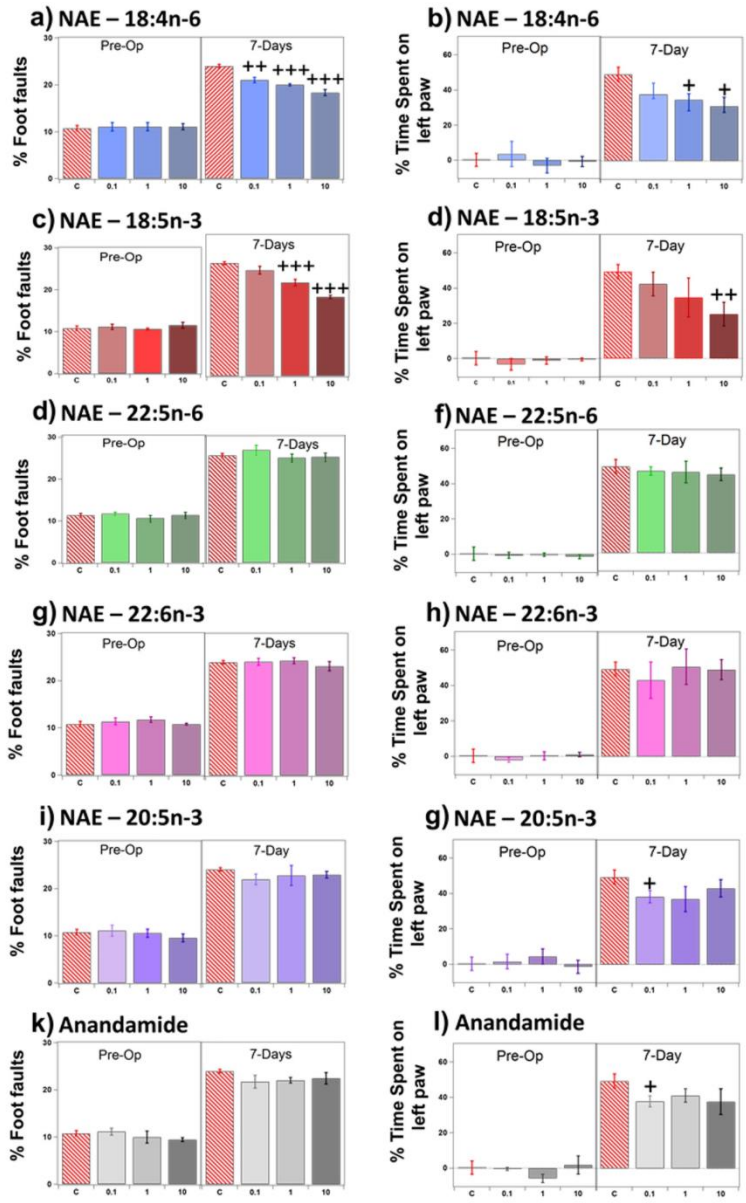

Fig. 5 Behavioral recovery assessment in young mice following photothrombosis stroke using grid walking / forelimb function (left, percent foot faults relative to total steps taken) and cylinder / forelimb asymmetry tasks (right, percent time spent on left paw relative to the right paw, a zero value on the cylinder task indicates that the animal spends equal amounts of time on each paw). Data are shown as mean ± s.e.m. + = P≤0.05, ++ = P≤0.01, +++ = P≤0.001 compared to stroke + vehicle controls

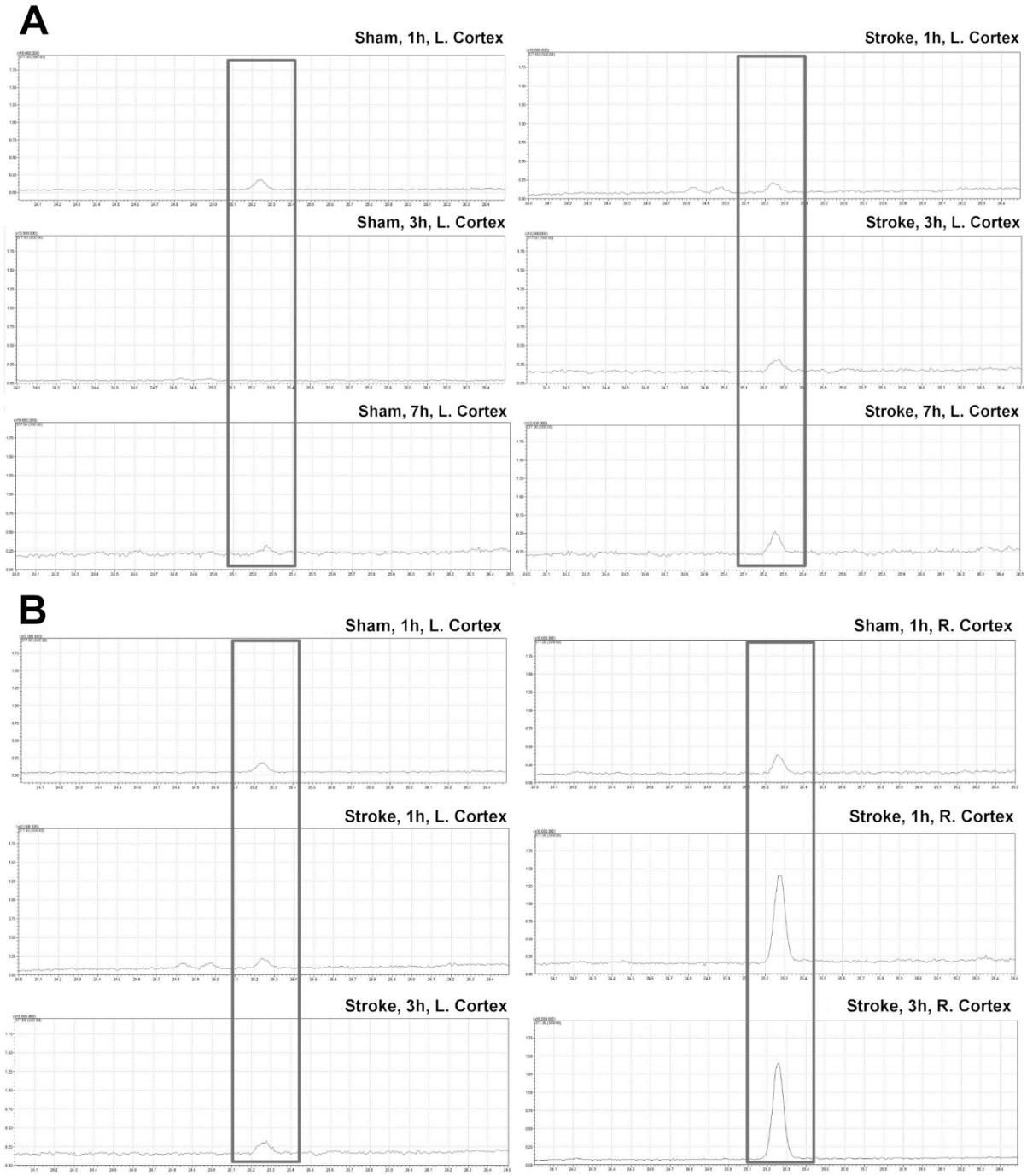

Fig. 6 A (top): Left cortex of sham/normal *vs.* stroke model – SIM GCMS analysis of mouse brain tissue following intranasal administration of ^{13}C labelled NAE-18:4n-6 after 1, 3 and 7 hours. B (bottom): Left cortex *vs*. right cortex – SIM GCMS analysis of mouse brain tissue following intranasal administration of ^{13}C labelled NAE-18:4n-6 after 1 and 3 hours *vs*. sham/normal brain

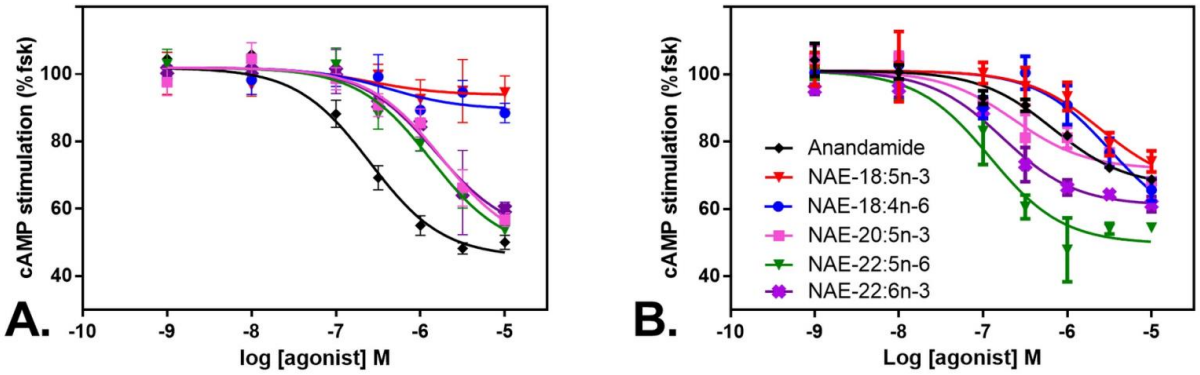

Fig. 7 A: Function at hCB_1 receptor with a cAMP assay inhibition of forskolin stimulated cAMP by the NAE tested (performed in duplicate, n=3). B: Function at hCB2 receptor with a cAMP inhibition of forskolin stimulated cAMP by NAE tested (n=5)